Midtropospheric frontogenesis associated with antecedent indirect precipitation ahead of tropical cyclones over the Korean Peninsula

By EUN-HYUK BAEK[1], JOO-HONG KIM[1]*, JONG-SEONG KUG[2] and GYU-HO LIM[3], [1]*Korea Polar Research Institute, 26 Songdomirae-ro, Yeonsu-gu, Incheon 406-840, South Korea*; [2]*Pohang University of Science and Technology, Pohang, South Korea*; [3]*School of Earth and Environmental Sciences, Seoul National University, Seoul, South Korea*

ABSTRACT

On the Korean Peninsula (KP), heavy rainfall often precedes the landfall of a tropical cyclone (TC). This rainfall is called antecedent indirect precipitation (AIP), because it occurs well beyond the effective radius of the TC. The present study examines the statistical characteristics and physical mechanism of the AIP produced by TCs that influenced the KP during the period 1993–2004. Composite analyses demonstrate that the AIP events were accompanied by midtropospheric frontogenesis due to the TC-mid-latitude environment interaction. When an approaching TC encountered an approaching mid-latitude upper-level trough, this encounter resulted in confluent and deformed flows at the mid-level by the combination of westerlies from the trough and southerlies from the TC. The delicate balance of horizontal winds related to the two systems at the mid-level led to the midtropospheric frontogenesis to the north of the KP. The frontogenetic feature related to the AIP was in marked contrast to those of the remote rainfall event over the KP and the predecessor rainfall event over the United States suggested by previous studies. Quasi-geostrophic analysis demonstrates that the midtropospheric front induced thermally direct circulation, which led to ascending motion over the KP. Consequently, the midtropospheric front helped to intensify the AIP, together with the convective instability that was amplified by the transport of warm and moist air along the conduit between the TC and subtropical high.

Keywords: tropical cyclone, antecedent indirect precipitation, TC–mid-latitude interaction, QG frontogenesis, remote rainfall, predecessor rainfall event

1. Introduction

Extratropical synoptic-scale waves preferentially develop and traverse East Asia to the mid-latitude western North Pacific basin, where the atmospheric environment is highly baroclinic all year round in association with the jet-stream. Climatologically, about one-third of all tropical cyclones (TCs) undergo recurvature over the western North Pacific (Archambault et al., 2013). When TCs recurve and proceed to mid-latitudes, they usually encounter baroclinic waves and actively interact with them. During the interaction, a rainfall event frequently occurs poleward of the TC. This type of TC-related rainfall has been named variously in different studies; for example, predecessor rainfall event (PRE; e.g. Galarneau et al., 2010; Schumacher et al., 2011; Bosart et al., 2012; Moore et al., 2013), remote rainfall (RR;

e.g. Wang et al., 2009; Chen et al., 2010; Byun and Lee, 2012), or antecedent (indirect) precipitation (e.g. Baek et al., 2013, 2014).

Such events from a large number of TCs in the North Atlantic have been analysed. Stohl et al. (2008) described an extreme precipitation event on the Norwegian southwest coast that was triggered by the transport of tropical moisture to the region ahead of two TCs. Galarneau et al. (2010) defined the PRE as a heavy rainfall event over the United States (US) that occurs well in advance of a recurving TC. They showed the PRE's synoptic characteristics and noted that deep tropical moisture is transported well poleward of a TC, which is forced to ascend when encountering a pre-existing low-level baroclinic zone associated with low-level frontogenesis. They found that during 1995–2008, approximately 30% of all North Atlantic TCs that passed west of 70°W and north of 20°N produced at least one PRE. Schumacher et al. (2011) quantified the effect of tropical moisture from TC Erin (2007) on the PRE by removing the

*Corresponding author.
email: jhkim004@gmail.com

1

moisture source in the initial condition of a numerical model simulation. Moore et al. (2013) classified the PREs into three categories (i.e. 'jet in ridge', 'southwesterly jet' and 'downstream confluence'), based upon the configuration of synoptic-scale upper-level flows during the PRE development. Although the three categories have common characteristics that are consistent with those identified by Galarneau et al. (2010), they are different with respect to the phasing of a TC with the synoptic-scale flow and to their interactions.

In the western North Pacific, similar rainfall events have occurred persistently over China, Japan and the Korean Peninsula (KP) in advance of TCs. Chen et al. (2010) classified the precipitation patterns related to landfalling TCs in China into five categories according to precipitation regions with respect to synoptic features. Among the categories, heavy rainfall downstream of the mid-latitude trough was called 'remote rainfall (RR)'. Based on a case study of Typhoon Songda (2004), Wang et al. (2009) demonstrated that moisture transport from the TC enhanced RR in southern Japan and its adjacent seas when the TC was passing far (i.e. $> 1200\,\mathrm{km}$) from the precipitation region. Over the KP, Byun and Lee (2012) showed through composite analyses of 46 TC cases that the RR events (RREs) have similar characteristics to the US events identified as PREs. In their study, when surface frontogenesis occurs at the equatorward side of an upper-level jet over the KP, RR is triggered with the aid of the transport of tropical moisture by a TC.

Meanwhile, Baek et al. (2013, 2014) scrutinised two representative cases [i.e. Typhoons Rusa (2002) and Maemi (2003)] having clear double precipitation peaks over the KP, yet these cases were not identified as RREs by Byun and Lee (2012). The first precipitation events of these peaks occurred outside the TCs' effective radius,[1] and their moisture sources were transported by the TC-related southerlies. Based on these characteristics, those events might be merely regarded as omitted cases of RR, but they were not so because of a notable difference in terms of the frontogenetic aspect. It was the occurrence of *midtropospheric frontogenesis*, rather than near-surface frontogenesis, generated by the interaction between the TC and mid-latitude trough. This important difference led us to distinct those events from the RREs, so we called them indirect precipitation (Baek et al., 2013) or antecedent rainfall (Baek et al., 2014). To standardise the terminology, the relevant events are rechristened as antecedent indirect precipitation (AIP) hereafter.

Although the two studies demonstrated midtropospheric frontogenesis in association with the AIP events, the results just from the two cases cannot be generalised. More cases need to be identified to determine whether midtropospheric frontogenesis is typically associated with AIP. As such examples, Fig. 1 shows three additional cases – Bart (1999), Saomai (2000) and Soudelor (2003). Although the observed precipitation events over the KP for these cases were not identified by Byun and Lee (2012), the events clearly occurred beyond the effective radius of each TC, resulting in double precipitation peaks in the time series of hourly precipitation at the surface station recorded maximum precipitation in South Korea. The identification of more cases naturally led to the necessity of new categorisation of TC-related precipitation over the KP, that is, the AIP event.

In this study, all the TCs that affected the KP from 1993 to 2004 are examined based on the 'Typhoon White Book (2011)' issued by the Korea Meteorological Administration (KMA). Among them, the AIP events are collected based on the new categorisation and are investigated with respect to their statistical characteristics. Following Baek et al. (2013, 2014), which emphasised midtropospheric frontogenesis as a distinctive phenomenon associated with the AIP over the KP, here we aim to generalise the relevant frontogenetic features occurred due to confluent and deformed flows between westerlies from an upper-level trough and southerlies from a TC. Composite analyses with all selected AIP cases identified would enable us to generalise the AIP event over the KP and to compare it with the RRE (Byun and Lee, 2012) and the PRE (Moore et al., 2013). Accordingly, this study seeks answers to the following questions:

(1) How can the AIP event be categorised?
(2) How often are TCs that affect the KP accompanied by the AIP event?
(3) How does the synoptic environment of the AIP cases differ from that of the non-AIP cases?
(4) Is midtropospheric frontogenesis observed for the AIP cases a result of the TC–mid-latitude trough interaction?
(5) How does the physical process of frontogenesis affect AIP?
(6) Is the frontogenetic feature of the AIP cases indeed in marked contrast to those of the RRE and PRE cases?

This article is organised as follows: Section 2 provides the data and methods. Section 3 provides a description of case identification for categorisation of AIP and statistical characteristics of the AIP cases in comparison to those of the non-AIP cases. Section 4 provides detailed analyses of midtropospheric frontogenesis and its connection to AIP,

---

[1]Effective radius is defined as a radius directly influenced by TC. We will discuss the arithmetical definition in Section 3.
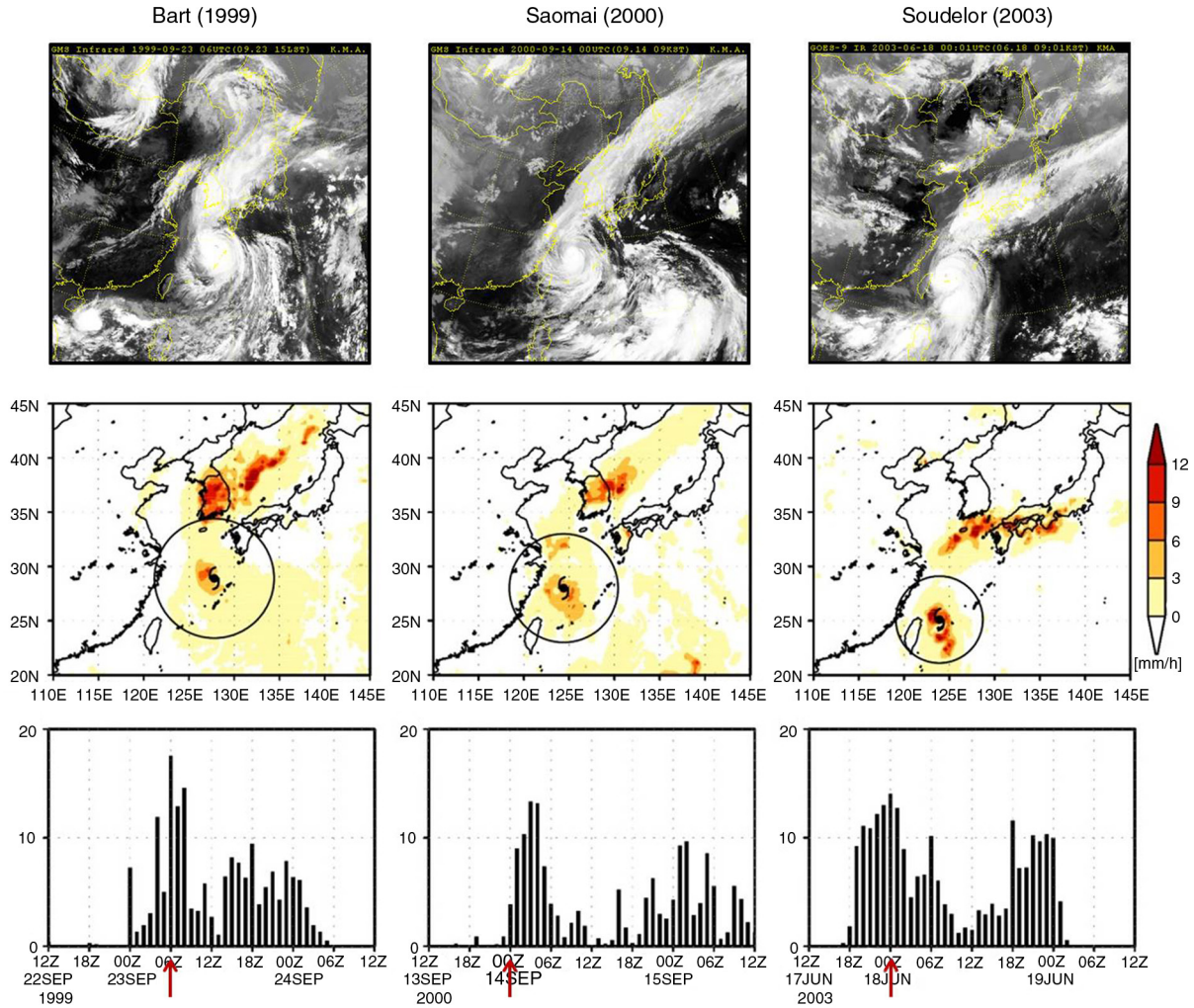
Fig. 1. IR images from the GMS (upper panels) and rain rates (units: mm h^{-1}) from the Tropical Rainfall Measuring Mission (TRMM) 3B42 V6 data together with the effective radius of TC (middle panels) at the peak time of the first rainfall (red arrows in the bottom panels). The bottom panels show the time series of hourly precipitation from surface station recorded maximum precipitation in South Korea during the period associated with the TCs for the three AIP cases: Bart (1999; left), Saomai (2000; middle) and Soudelor (2003; right).

and Section 5 discusses comprehensive interpretation of the process of AIP and comparison with other studies. Section 6 discusses dynamic interpretation of midtropospheric frontogenesis. Finally, Section 7 gives summary and concluding remarks.

2. Data and methods

2.1. Data sets

The 'Typhoon White Book (2011)' issued by the KMA gives information on the TCs that influenced the KP from 1904 to 2010, such as the maximum wind speed and direction, maximum daily precipitation and accumulated precipitation at surface stations as well as the TC tracks (available via www.typ.kma.go.kr/TYPHOON/pds/pds_03_1.jsp).

In this study, we examine the 41 TCs that influenced the KP from 1993 to 2004. The period chosen is limited by the availability of station-based hourly precipitation data. The hourly precipitation data at 57 surface stations (Fig. 2) in South Korea are used to analyse rainfall induced by approaching TCs. The 6-hourly accumulated precipitation is calculated at time steps centred at 00, 06, 12 and 18 UTC.

The best-track data used are the archives of the Regional Specialized Meteorological Center (RSMC) Tokyo–Typhoon Center. The RSMC best-track data provide centre positions, minimum central pressures, maximum sustained wind speeds and radii of wind speed ≥ 30 knots (~ 15.4 m s^{-1}), among other TC properties at 6 h intervals. The interval is shortened to 3 h when a TC is in close proximity to Japan, but here only the data at 00, 06, 12 and 18 UTC are used to
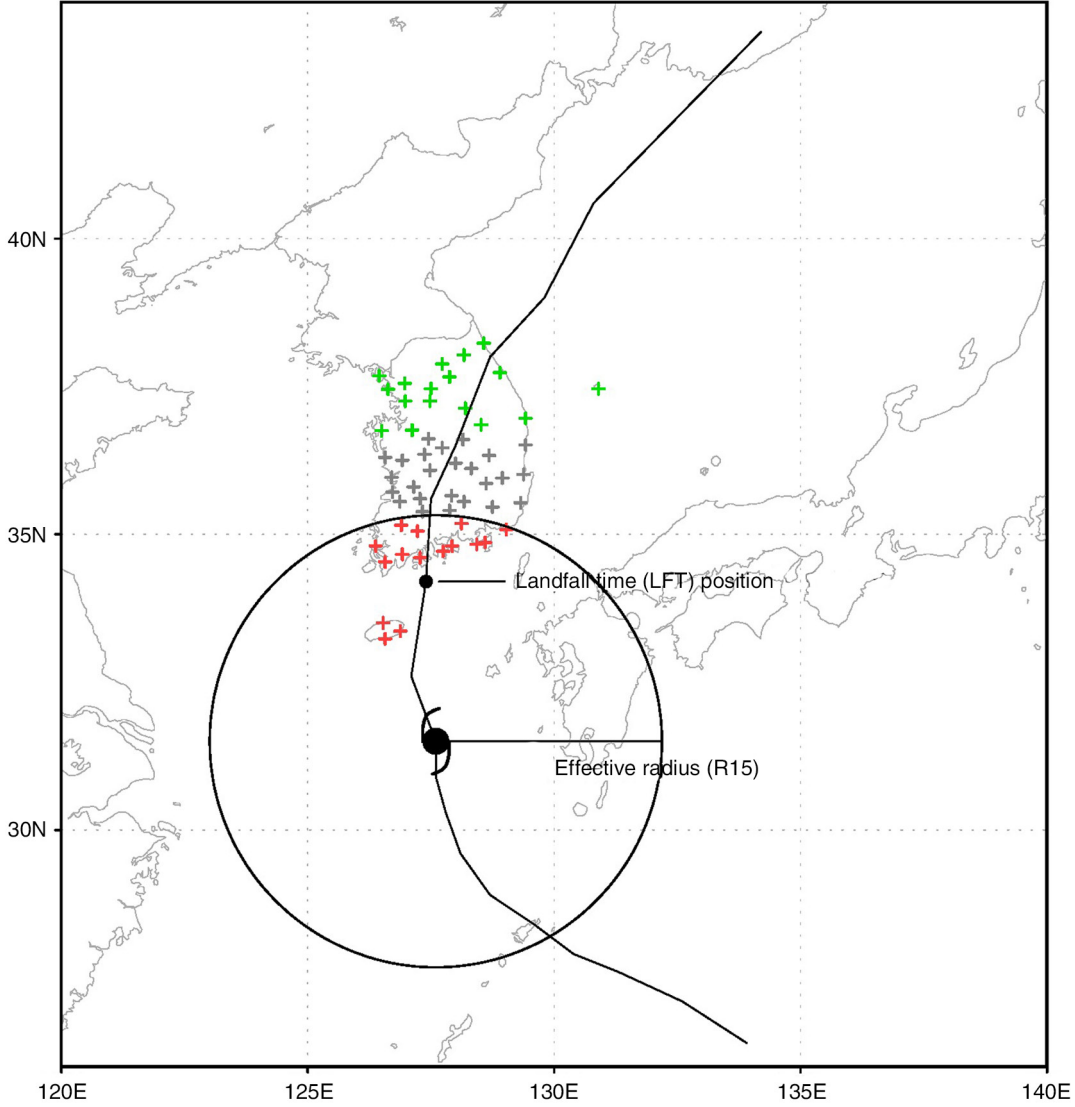
Fig. 2. Schematic of effective radius (R15) of TC, effective landfall time (LFT) and the station locations for direct precipitation (red crosses) and AIP (green crosses). Grey crosses denote the stations with no precipitation. Black line denotes TC track.

synchronise the analysis time with the re-analysis data and the station-based 6-hourly accumulated precipitation data.

The Japanese 25-year Re-analysis (JRA-25) data are used to diagnose the synoptic environment (Onogi et al., 2007). The horizontal resolution of the JRA-25 is $1.25°$ in both latitude and longitude. The data are provided on 23 standard pressure levels from 1000 to 10 hPa. The data cover the period from 1979 to the present at 6 h intervals. The JRA-25 data have many advantages for studying TC-related phenomena because it is produced with data assimilation of TCs' wind profiles reconstructed from historical best-track information (Onogi et al., 2007). In addition, infrared images from the Geostationary Meteorological Satellites GMS-4 and GMS-5 are used to examine features related to large-scale clouds.

2.2. *Diagnostic methods*

The quasi-geostrophic (QG) theory is applied to examine the role of midtropospheric frontogenesis in ascending motion for the AIP cases. The QG frontogenesis function (Martin, 2006) is

$$
F_g = \frac{d_g}{dt}|\nabla_p \theta| = \frac{1}{|\nabla_p \theta|}\left[-\frac{\partial \theta}{\partial x}\left(\frac{\partial u_g}{\partial x}\frac{\partial \theta}{\partial x} + \frac{\partial v_g}{\partial x}\frac{\partial \theta}{\partial y} \right) \\ -\frac{\partial \theta}{\partial y}\left(\frac{\partial u_g}{\partial y}\frac{\partial \theta}{\partial x} + \frac{\partial v_g}{\partial y}\frac{\partial \theta}{\partial y} \right) \right],
\tag{1}
$$

where $\frac{d_g}{dt} = \frac{\partial}{\partial t} + u_g\frac{\partial}{\partial x} + v_g\frac{\partial}{\partial y}$.

Equation (1) can be rewritten in Q-vector form:

$$F_g = \left(\frac{1}{f\gamma}\right)\frac{1}{\nabla_p\theta}\vec{Q}\cdot\nabla_p\theta, \qquad (2)$$

where

$$\begin{aligned}\vec{Q} &= f\gamma\frac{d_g}{dt}\nabla_p\theta \\ &= f\gamma\left[-\left(\frac{\partial u_g}{\partial x}\frac{\partial\theta}{\partial x}+\frac{\partial v_g}{\partial x}\frac{\partial\theta}{\partial y}\right), -\left(\frac{\partial u_g}{\partial y}\frac{\partial\theta}{\partial x}+\frac{\partial v_g}{\partial y}\frac{\partial\theta}{\partial y}\right)\right]\end{aligned}$$

and

$$\gamma = \frac{R}{fp_o}\left(\frac{p_o}{p}\right)^{c_v/c_p}.$$

Equation (2) indicates that any place where Q-vectors point across the isentropes from cold to warm air will be associated with horizontal frontogenesis (i.e. $F_g > 0$), that is a positive value of F_g implies that the Q-vectors are oriented towards the warm side of a frontogenetical region, which also tells us that the frontogenesis leads the convergence of Q-vectors on the warm side of the front and the divergence of the vectors on its cold side. Consequently, QG frontogenesis induces thermally direct circulation (e.g. Martin et al., 1992).

Each term of the QG omega equation is also calculated to quantitatively assess the degree to which the QG frontal forcing affects ascending motion on the rainfall region. For a frictionless atmosphere, the QG omega equation is

$$\begin{aligned}\left(\nabla^2 + \frac{f_0^2}{\sigma}\frac{\partial^2}{\partial p^2}\right)\omega = &-\frac{f_0}{\sigma}\frac{\partial}{\partial p}\left[-\vec{V}_g\cdot\nabla\left(\frac{1}{f_0}\nabla^2\Phi+f\right)\right] \\ &-\frac{1}{\sigma}\nabla^2\left[-\vec{V}_g\cdot\nabla\left(-\frac{\partial\Phi}{\partial p}\right)\right] \\ &-\frac{R}{\sigma_p}\nabla^2\left(\frac{1}{C_p}\frac{dQ}{dt}\right).\end{aligned} \qquad (3)$$

The right-hand side of eq. (3) includes three forcing terms, which represent the differential geostrophic vorticity advection, the Laplacian of potential temperature advection and the Laplacian of diabatic heating, respectively. In the third term, the diabatic heating can be computed as a residual of the thermodynamic equation. However, the calculation of Eulerian derivatives using the JRA-25 data with 6 h time intervals yields large computational residuals because of the coarse temporal resolution of the data (Moore and Montgomery, 2005). To avoid this problem, computing the diabatic heating from 3-D air parcel trajectories has been proposed to minimise the computational error (e.g. Galarneau et al., 2009; Cordeira and Bosart, 2011). Baek et al. (2013) used this Lagrangian method to calculate the diabatic heating term in the frontogenesis

function as follows: the 6-hourly data are linearly interpolated to 1 h intervals, then the Lagrangian derivative of potential temperature at a grid point is computed using the centred finite difference method. We follow this method to obtain the diabatic heating in eq. (3).

3. AIP: its identification, statistical properties and synoptic background

3.1. Comparison of AIP with RRE

As mentioned in Section 1, both Byun and Lee (2012) and Baek et al. (2013, 2014) have addressed the TC-related distant precipitation over the KP when the direct rainbands of the TC did not reach the KP. Byun and Lee (2012) collected 46 TC cases that brought about the RREs over the KP. The collected cases were divided into two groups: one includes the events related to the landfalling TCs over China (RR-LT cases) and the other is related to the recurving TCs traversing the East China Sea (RR-OT cases; see Fig. 4 in Byun and Lee, 2012). Similar to the RR-OT cases, the two distant precipitation (what we call AIP here) events introduced in Baek et al. (2013, 2014) occurred while the associated TCs were located over the East China Sea. Commonly noted features are that the moisture transport from the TC provides the source of precipitation and destabilises the lower troposphere over the precipitating region. With these points only, it could be said that the two AIP cases are nothing different from the RR-OT cases. However, we think that the AIP events deserve to be distinguished from the RR-OT cases, not only because they were not included in Byun and Lee (2012) due to the chosen distance criterion between the TC and the precipitating region but also because of the notable difference in the frontogenetic feature. In short, Byun and Lee (2012) proposed pre-existing surface frontogenesis as the updraft forcing of convection, whereas Baek et al. (2013, 2014) demonstrated the occurrence of midtropospheric frontogenesis by the interaction between the TC and mid-latitude trough and the resultant intensification of the ascent on the warm side of the front.

Before investigating the statistical characteristics and the general mechanism associated with the AIP event, it would be informative for us to compare between the typical RR-OT and AIP cases. Figure 3 compares the synoptic background and QG frontogenesis function between the RR-OT case – Nari (2007) and the AIP case – Saomai (2000) at the time of maximum precipitation.[2] In the typical RR-OT case,

---

[2]Byun and Lee (2012) presented the initial time (t0) of the RREs in their article. In the Typhoon Nari (2007) case shown in Fig. 3, the time of maximum precipitation is set at t0+12 h based on the analysis of hourly station precipitation data.
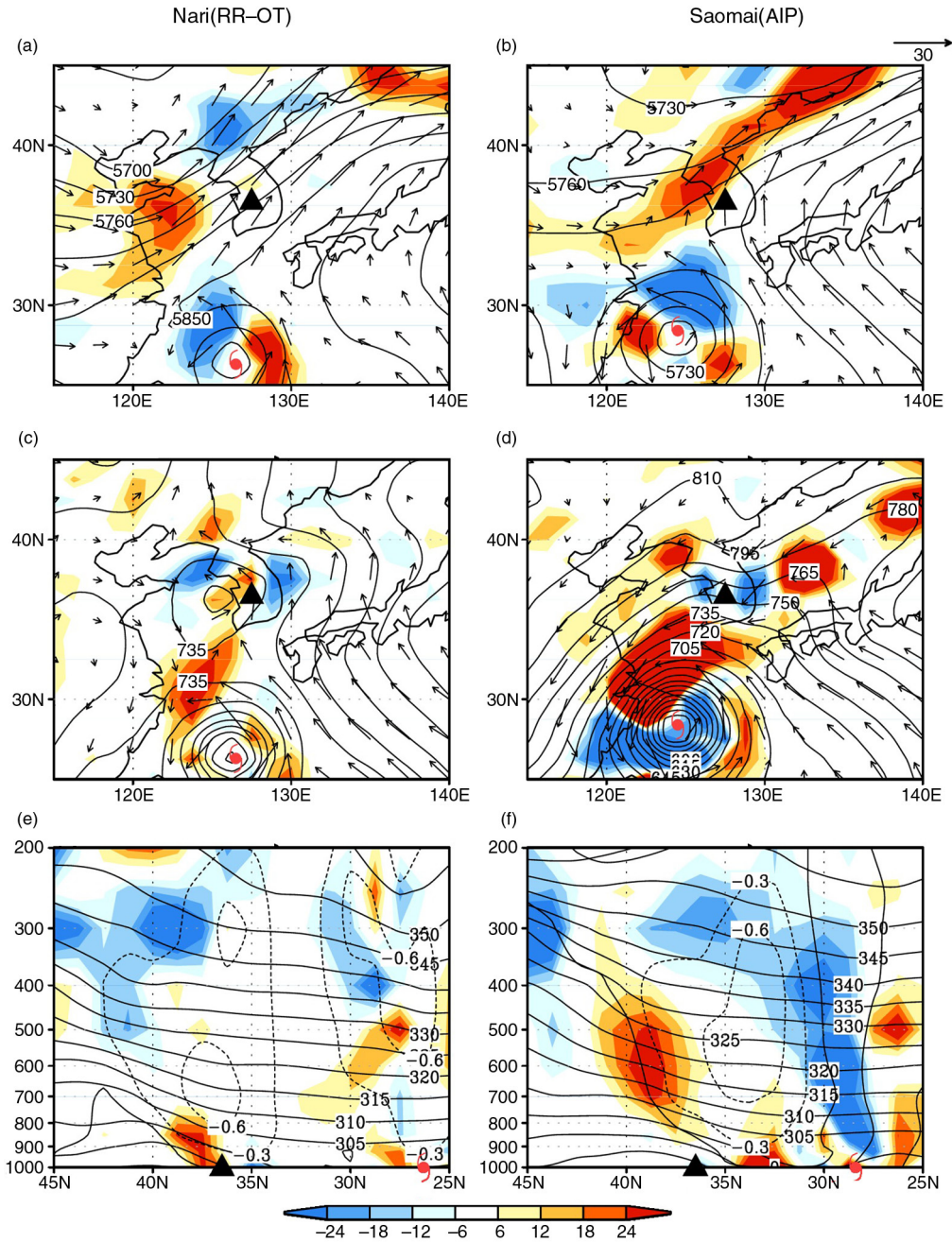
Fig. 3. Geopotential height (contour, units: gpm), QG frontogenesis [shading, units: 10^{-11} K (m s)$^{-1}$] and horizontal winds (vector, units: m s^{-1}) at (a, b) 500 hPa, and (c, d) 925 hPa and (e, f) the meridional–vertical cross-section of QG frontogenesis, potential temperature (thick contour, units: K) and pressure velocity (thin contour, units: Pa s^{-1}) along 127.5°E at the maximum precipitation time for the representative two cases of RR-OT (Nari, 2007; left panel) and AIP (Saomai, 2000; right panel), respectively. The black triangle and TC symbol indicate the precipitating region and composite TC location, respectively.

midtropospheric frontogenesis does not appear over the KP, though the rainfall region locates downstream of the upper-level trough (Fig. 3a). In the lower troposphere, however, a pre-existing surface low-pressure system intrudes into the KP with an accompanying surface warm front down-

stream of the surface low (Fig. 3c). The surface frontogenesis seems to enhance the RRE over the KP as an updraft forcing of deep convection as described by Byun and Lee (2012). These features are shown well in the meridional-vertical cross-section at 127.5°E (Fig. 3e). The RR region
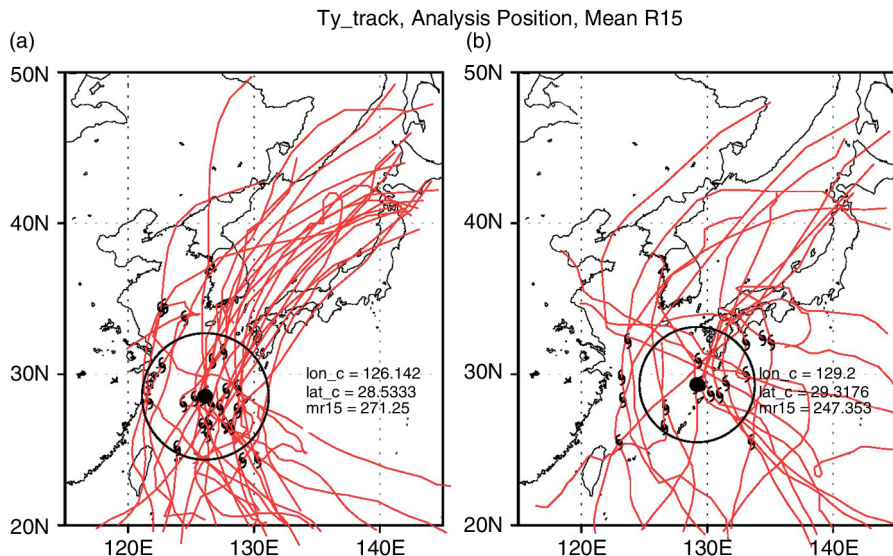
Ty_track, Analysis Position, Mean R15

Fig. 4. Locations (black TC symbols) and tracks (red line) of the TCs at the analysis time for (a) the AIP and (b) non-AIP cases. The black point and black circle denote mean location and mean effective size for each case, respectively.

locates on the warm side of surface frontogenesis where deep convection occurs apart from the TC.

In contrast, the typical AIP case shows that the southwest–northeast oriented distant frontogenesis occurs at the midtroposphere (Fig. 3b). The confluent deformation flows are induced over the KP between the westerlies from the upper-level trough and the southerlies from the TC at the midtroposphere. The flows lead to strong midtropospheric frontogenesis similar to the two cases of Baek et al. (2013, 2014). In the low level, although there are several strong areas of surface frontogenesis, none of them appear to directly contribute to the updraft motion at the precipitating region over the KP (Fig. 3d). In the cross-section, it is shown that the midtropospheric front at nearby north of the AIP region contributes to the updraft motion apart from the TC (Fig. 3f). The difference in the frontogenetic features associated with the distant precipitation over the KP ahead of a TC leads us to attempt to examine the general characteristics of the AIP events.

3.2. Case identification

RR or AIP ahead of TC has not yet been defined objectively. Galarneau et al. (2010) defined the PRE based on the radar images and moisture advection associated with TCs approaching the US. However, radar data over the seas that surround the KP are not available. Byun and Lee (2012) defined the separation distance between the TC and RR region (i.e. critical radius) as a sum of (1) the longest radius of $15.4 \, \mathrm{m \, s^{-1}}$ winds, (2) the maximum radius of the rain fields induced by the TC itself and (3) the 6-hourly moving distance of TC. In their study, the mean

distance between the RR region and the TC centre was $\sim 1540 \, \mathrm{km}$, which is longer than that used to define the PRE examined by Galarneau et al. (2010) (i.e., $\sim 1000 \, \mathrm{km}$). The long critical radius could cut off many AIP cases, which show a distinct precipitation from that around TC.

Baek et al. (2013, 2014) suggested a practical definition of AIP over the KP as to be the precipitation recorded at the surface stations located farther than the effective radius of TC (Fig. 2). They simply defined the effective radius of TC as the information on the longest radius of $15.4 \, \mathrm{m \, s^{-1}}$ wind (R15), provided by the RSMC data set (Fig. 2). Here, we introduce a concept of antecedent time associated with TC as the period from 48 to 12 h before the TC's effective landfall time.[3] If precipitation over the KP occurs before the antecedent time, it is hard to consider the precipitation to be associated with TC. With the criteria of location and time, we classify the 41 TC cases affecting the KP into two groups depending on the presence of AIP. A TC would be classified as the AIP case if at least one station in South Korea recorded maximum 6 h precipitation $> 40 \, \mathrm{mm}$ outside of the effective radius of the TC during its antecedent time. The value of $40 \, \mathrm{mm} \, (6 \, \mathrm{h})^{-1}$ is based on the heavy rain advisory $[80 \, \mathrm{mm} \, (12 \, \mathrm{h})^{-1}]$ of the KMA. Otherwise, a TC is classified as the non-AIP case. According to this definition, 23 TCs among them can be classified as the AIP cases (Table 1) and the remaining 18 TCs as the non-AIP cases (Table 2). Byun and Lee (2012) collected 16 TC cases as the RRE during the same period, among

---

[3]The effective landfall time is defined as the time when a TC makes its landfall on the KP or it is located at the nearest position from the shore.

Table 1.   List of all documented AIP cases over the KP from 1993 to 2004

			AIP – 23 cases			
Year	TC name	LFT	T0	Precip	Stn	Diff
1993	PERCY	18Z29JUL	00Z29JUL	129	Suwon	18
1993	ROBYN	00Z10AUG	06Z08AUG	145	Jecheon	42
1993	YANCY	12Z03SEP	06Z02SEP	52	Seoul	30
1994	DOUG	06Z11AUG	12Z10AUG	90	Sokcho	30
1995	FAYE	06Z23JUL	06Z22JUL	110	Jeju	24
1995	JANIS	12Z26AUG	18Z24AUG	265	Boryeong	42
1995	RYAN*	18Z23SEP	00Z23SEP	109	Sokcho	18
1996	KIRK	00Z14AUG	12Z12AUG	72	Gwangju	36
1997	TINA	18Z08AUG	00Z07AUG	99	Mokpo	42
1998	YANNI*	06Z30SEP	18Z29SEP	103	Geoje	12
1999	OLGA	00Z03AUG	06Z02AUG	190	Yeongju	18
1999	ANN	12Z20SEP	12Z19SEP	159	Sanchoen	24
1999	BART	00Z24SEP	06Z23SEP	86	Uljin	18
2000	KAI-TAK	06Z11JUL	12Z10JUL	138	Haenam	18
2000	SAOMAI	18Z15SEP	00Z14SEP	72	Seosan	42
2002	RUSA	06Z31AUG	18Z30AUG	120	Gangneung	12
2003	LINFA*	00Z31MAY	18Z29MAY	88	Jangheung	30
2003	SOUDELOR	06Z19JUN	00Z18JUN	88	Seogwipo	30
2003	ETAU*	06Z08AUG	00Z07AUG	70	Cheonan	30
2003	MAEMI	12Z12SEP	18Z11SEP	142	Goheung	18
2004	MINDULLE	12Z04JUL	12Z03JUL	155	Gwangju	24
2004	MEGI	00Z19AUG	00Z18AUG	208	Jangheung	24
2004	SONGDA	00Z07SEP	00Z06SEP	46	Ulleungdo	24
	Average			116.5		26.5

LFT: landfall time (see footnote in the text), T0: analysis time, Precip: maximum 6 h precipitation at the analysis time [units: mm $(6\,h)^{-1}$], Stn: surface station at which maximum precipitation was recorded, Diff: time difference between LFT and T0 (units: h). The asterisk marks cases shared with remote rainfall cases suggested by Byun and Lee (2012).

which 7 TCs are RR-LT cases and 9 TCs are RR-OT cases, respectively. Among the RR cases, four TCs – Ryan (1995), Yanni (1998), Linfa (2003) and Etau (2003) – are common with AIP identified by this study.

3.3. Statistical properties

The AIP cases occurred more frequently ($\sim 56\%$) than the non-AIP cases among the 41 TCs affecting the KP during 1993–2004. This fact reveals that the AIP event should be considered a likely scenario in forecasting the precipitation associated with a TC approaching to the KP. Analysis time of each AIP case is set at the time when the amount of 6 h precipitation is the largest during the antecedent time. On average, the maximum 6 h precipitation reached 116.5 mm $(6\,h)^{-1}$ (Table 1), which exceeds the KMA's heavy rain advisory of 80 mm $(12\,h)^{-1}$. The average gap between the analysis and effective landfall time is about 27 h; that is, AIP tends to occur about 1 d before a TC makes landfall on the KP. Thus, the analysis time of the non-AIP case is also chosen as 1 d before the effective landfall time to facilitate comparison between the two cases (Table 2). The AIP occurrence seems to have a seasonal preference (Table 3). Excluding May, June and October, for which sample sizes are too small to provide reliable statistical properties, the monthly frequency of AIP cases increased from July to September. This is because the activity of mid-latitude synoptic waves increases with the deepening of the trough around the KP from summer to autumn. That is, the AIP occurrence is highly associated with the synoptic environment that interacts with TCs.

Most TC tracks for the AIP (Fig. 4a) and non-AIP cases (Fig. 4b) recurve over the East China Sea. The pathways for the AIP cases are relatively similar to each other, whereas those for the non-AIP cases relatively spread out. At the analysis time, the TC centres of most AIP cases were concentrated around 28.5°N, which implies that the composite analysis is suitable for the AIP cases. The mean R15 is about 271 nautical miles (nm) for the AIP cases, and 247 nm for the non-AIP cases; that is, the TC sizes seem to be slightly larger for the AIP cases than for the non-AIP cases. It is noted that the KP is not included within the mean effective radius for the AIP cases; thus, any influence of the TCs on the rainfall events over the KP should not be direct.

Table 2. List of all documented non-AIP cases over the KP from 1993 to 2004

	Non-AIP – 18 cases		
Year	TC name	LFT	T0
1993	OFELIA	06Z27JUL	06Z26JUL
1994	WALT	00Z26JUL	00Z25JUL
1994	BRENDAN	00Z01AUG	00Z31JUL
1994	ELLIE	18Z13AUG	18Z12AUG
1994	SETH	18Z11OCT	18Z10OCT
1996	EVE	12Z18JUL	12Z17JUL
1997	ROSIE	00Z27JUL	00Z26JUL
1997	OLIWA	06Z16SEP	06Z15SEP
1998	ZEB	06Z17OCT	06Z16OCT
1999	NEIL	06Z27JUL	06Z26JUL
1999	PAUL	06Z07AUG	06Z06AUG
2000	BOLAVEN	00Z31JUL	06Z29JUL
2000	PRAPIROON	12Z31AUG	12Z30AUG
2002	RAMMASUN	00Z06JUL	00Z05JUL
2002	NAKRI	12Z13JUL	12Z12JUL
2002	FENGSHEN	12Z26JUL	12Z25JUL
2004	NAMTHEUN	00Z01AUG	00Z31JUL
2004	CHABA	06Z30AUG	06Z29AUG

TC name: parent TC of the non-AIP case; LFT: effective landfall time; T0: analysis time.

3.4. Composite synoptic background

To identify factors that led to the differences between the two cases, we compare their synoptic backgrounds. All fields are calculated for individual cases and then used to construct the composite fields of synoptic environments at 200, 500 and 850 hPa at the analysis time (Fig. 5). At 200 hPa, an upper-level trough is commonly observed over mainland China between 110 and 120°E (Fig. 5a and b), and this trough contributes to TC recurvature (Fig. 4). Compared to the non-AIP composite, however, the trough of the AIP composite is stronger, with a more intense and statistically more robust jet-stream reaching 40 m s^{-1}. Therefore, based on the thermal wind balance, the AIP cases have stronger baroclinicity than the non-AIP cases over the KP that is located east of the trough and equatorward of the jet-entrance. This positioning facilitates the synoptic-scale ascent that can organise convection and provide a favourable condition for the AIP event.

The composite fields of the AIP and non-AIP events have very different arrangement of the trough and subtropical high at the mid-level (Fig. 5c and d). For the AIP composite, the trough intrudes into the Yellow Sea and the westerlies of the pre-existing mid-latitude trough meet the southerlies between the TC and the subtropical high. This pattern produces a strong horizontal confluent field around the KP, and a relatively stronger temperature gradient appears at the same region. The interaction between the TC and mid-latitude trough for the AIP cases show a favourable environment for generating a frontal structure at the mid-level over the KP. By contrast, for the non-AIP composite, the trough remains in China and the subtropical high expands further to the KP. The confluent flow forms near Japan but is relatively weak, so the temperature gradient over the KP remains weak.

At the low level, the mid-latitude trough disappears in both composites (Fig. 5e and f). For the non-AIP composite, the anticyclonic ridge related to the subtropical high expands further towards the KP, compared to the AIP composite. As a result, the southerlies on the eastern periphery of TC do not extend to the KP (Fig. 5f). The predominant anticyclone over the KP hinders the northward transport of deep tropical moisture. By contrast, for the AIP composite, the low-level moist air accompanied by the southerlies on the east side of TC reaches the KP (Fig. 5e). The effective moisture transport between the TC and subtropical high is an important factor for the AIP occurrence over the KP, as suggested in previous research (e.g. Wang et al., 2009; Galarneau et al., 2010; Schumacher et al., 2011).

4. Midtropospheric frontogenesis for the AIP cases

The composite synoptic background of the AIP cases showed a favourable environment for generating a frontal structure at the mid-level (Fig. 5). In this section, we examine the composite fields of midtropospheric flow patterns, the frontogenetic features for the AIP cases so that we generalise the frontogenetic characteristics for the AIP cases, and then discuss how the front could form at the mid-level.

Table 3. Monthly occurrence numbers of AIP, non-AIP, and total cases and the monthly ratio of AIP to total (units: %)

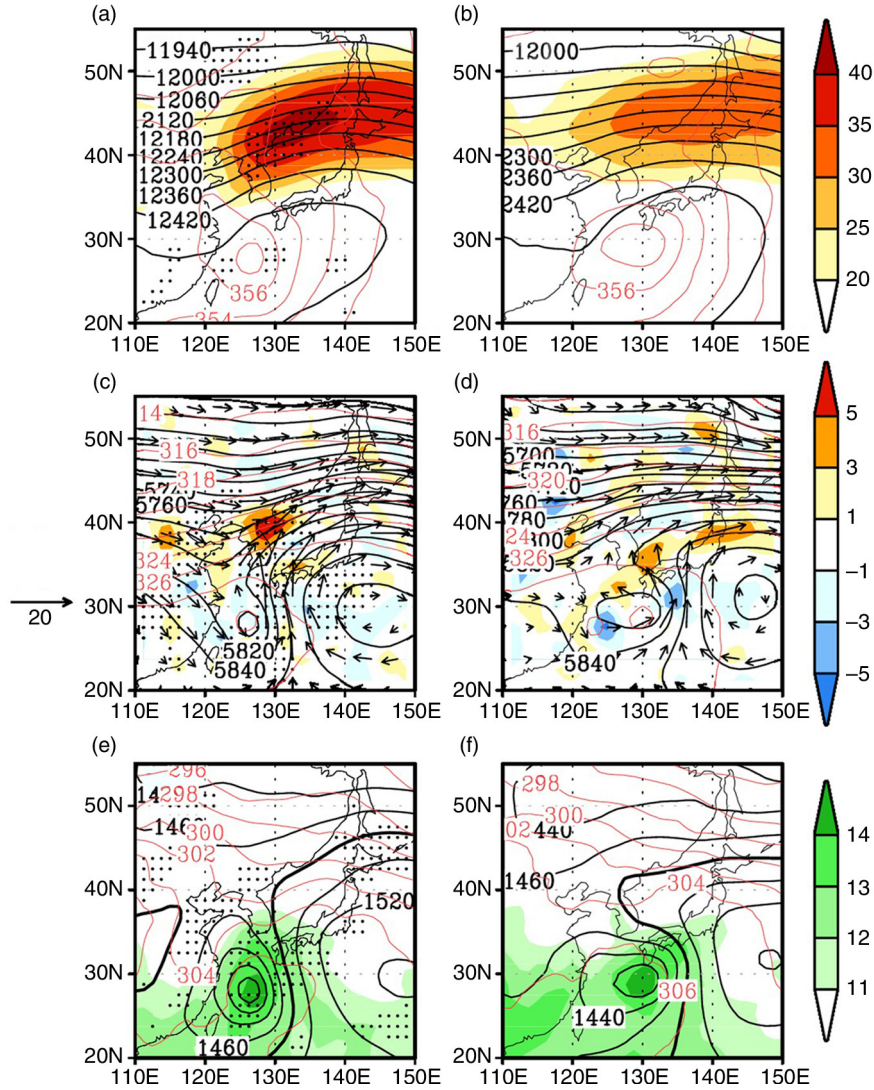|	May	Jun	Jul	Aug	Sep	Oct	Total
AIP	1	1	4	9	8	0	23
Non-AIP	0	0	11	4	1	2	18
Total	1	1	15	13	9	2	41
Ratio (AIP/total, %)	100	100	26.6	69.2	88.9	0	58.5

Fig. 5. Composite fields of geopotential height (black contour, units: gpm), temperature (red contour, units: K) at 200 hPa (a, b), 500 hPa (c, d) and 850 hPa (e, f) for the AIP (left panels) and non-AIP cases (right panels) at their respective analysis time. Shadings represent 200 hPa wind speed (units: m s^{-1}) in (a, b), 500 hPa horizontal winds (arrows, units: m s^{-1}) and convergence (units: 10^{-5} s^{-1}) in (c, d) and 850 hPa specific humidity (units: g kg^{-1}) in (e, f). Thick contours in (e, f) indicate the line at 1480 gpm. Dots denote the 90% significant region of the shading by the Student's *t*-test.

4.1. Midtropospheric frontogenesis

We have demonstrated that midtropospheric frontogenesis induced by the interaction between the TC and mid-latitude trough seems to be linked to AIP over the KP. To test whether this linkage actually occurs, the QG fronto-genesis function is calculated [eq. (1)]. It helps to examine how the TC–trough interaction contributes to the mid-tropospheric frontogenesis and to determine how the front influences AIP over the KP (Fig. 6a). For the composite analysis, the horizontal fields are calculated at individual levels and then vertically averaged between 700 and 400 hPa,

because the maximum frontogenesis levels slightly differ in the midtropospheric layers depending on cases. The mid-tropospheric streamline shows a typical synoptic pattern to form the midtropospheric front: that is, the mid-latitude trough to the north, the TC to the south and the subtro-pical high to the east. QG frontogenesis occurs as a result of confluent and deformed flows between the TC and mid-latitude trough. The existence of midtropospheric frontogenesis implies that ascending motion can be induced on the warm side of the front due to thermally direct circulation associated with the front (i.e. the AIP region). Two distinctive ascending regions are apparent: one in the
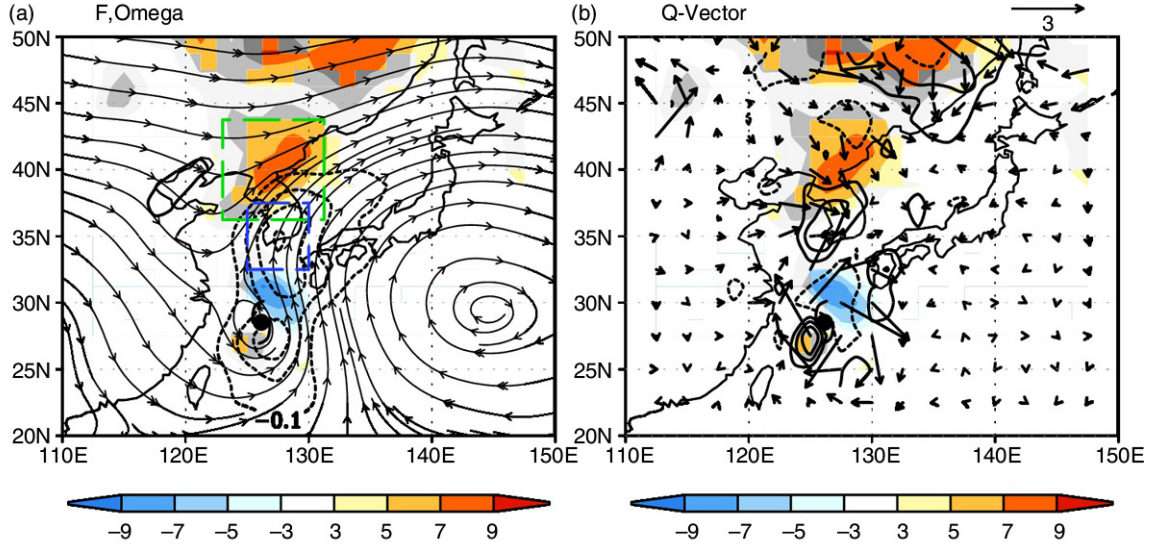
Fig. 6. Composite fields of (a) QG frontogenesis [shading, units: 10^{-11} K (m s)$^{-1}$], streamline and omega (contour, negative dashed, units: Pa s^{-1}) averaged between 700 and 400 hPa, and (b) $\vec{Q}\cdot\nabla_p\theta$ (shading, units: 10^{-16} K^2 m^{-2} s^{-1}), $\vec{Q}$ [vector, units: K (m s)$^{-1}$], $\vec{Q}$ convergence (contour, units: K m^{-2} s^{-1}) at the analysis time. The dashed green (blue) rectangular indicates the frontal (ascending) region, which will be used for area-average (see the text). Colour shadings denote the 90% significant region of the shading by Student's *t*-test. The TC symbol indicates the composite TC location.

east of the composite TC and the other on the warm side of the front over the KP. This pattern implies two important points: (1) the AIP event occurs indirectly, apart from the TC, and (2) the upward motion associated with AIP has a connection with the midtropospheric front induced by the interaction between the TC and mid-latitude trough. These features are consistent with the results of case studies on Rusa in 2002 and Maemi in 2003 (Baek et al., 2013, 2014).

The Q-vector is a useful tool to diagnose how QG frontogenesis leads to an ascent in the frontal region (Martin et al., 1997). From eq. (2), positive frontogenesis $\left(\frac{1}{|\nabla_p\theta|}\vec{Q}\cdot\nabla_p\theta\right)$ is consistent with a Q-vector pointing towards the warm side of the front (Fig. 6b). The QG forcing for the ascent, which is represented by the convergence of $\vec{Q}$ $\left(-\nabla\cdot\vec{Q}\right)$, apparently occurs on the warm side of the front over the KP. The distribution of this forcing reveals that the region with midtropospheric QG forcing between the TC and trough is in good agreement with the ascending region over the KP, although the centre of the convergent region is slightly shifted to the west from the centre of the ascending region. The considerable amounts of the $\vec{Q}$ convergence over the KP possibly indicate that at least within the KP, the contribution of midtropospheric frontogenesis to the ascent is non-trivial. The area with the $\vec{Q}$ convergence is more compactly located over the KP than is the broad-scale ascending region.

4.2. Quantification of individual forcings contributing to the AIP-related upward motion

Naturally, not all ascending motions can be attributed to the QG forcing, because the intrusion of warm and moist air at the low and middle tropospheric layer also builds a convectively unstable environment supportive of deep convection. We calculate the QG omega equation of eq. (3) including the diabatic heating term (Fig. 7). This equation enables quantification of the distribution of upward motion related to the AIP. For the AIP composite, the QG omega equation represents the spatial pattern and magnitude of the omega quite well; that is, the 3-D Laplacian of composite omega on the left-hand side (LHS) of eq. (3) (Fig. 7a) is almost equal to the sum of geostrophic and diabatic forcings on the right-hand side (RHS) of the equation (Fig. 7b).

The vertical motion can be explained by a synergistic interaction between dynamics (i.e. QG forcing) and thermodynamics (i.e. convective heating). The sum of two of the QG forcing terms (i.e. the differential geostrophic vorticity advection and the Laplacian of potential temperature advection) describes the sum of spatial pattern of the $\vec{Q}$ convergence (Fig. 6b) and the β effect:

$$-f_0\frac{\partial}{\partial p}\left[-\vec{V}_g\cdot\nabla\left(\frac{1}{f_0}\nabla^2\varphi+f\right)\right]$$
$$-\nabla^2\left[-\vec{V}_g\cdot\nabla\left(-\frac{\partial\varphi}{\partial p}\right)\right]=-2\nabla\cdot\vec{Q}+f_0\beta\frac{\partial v_g}{\partial p}. \tag{4}$$

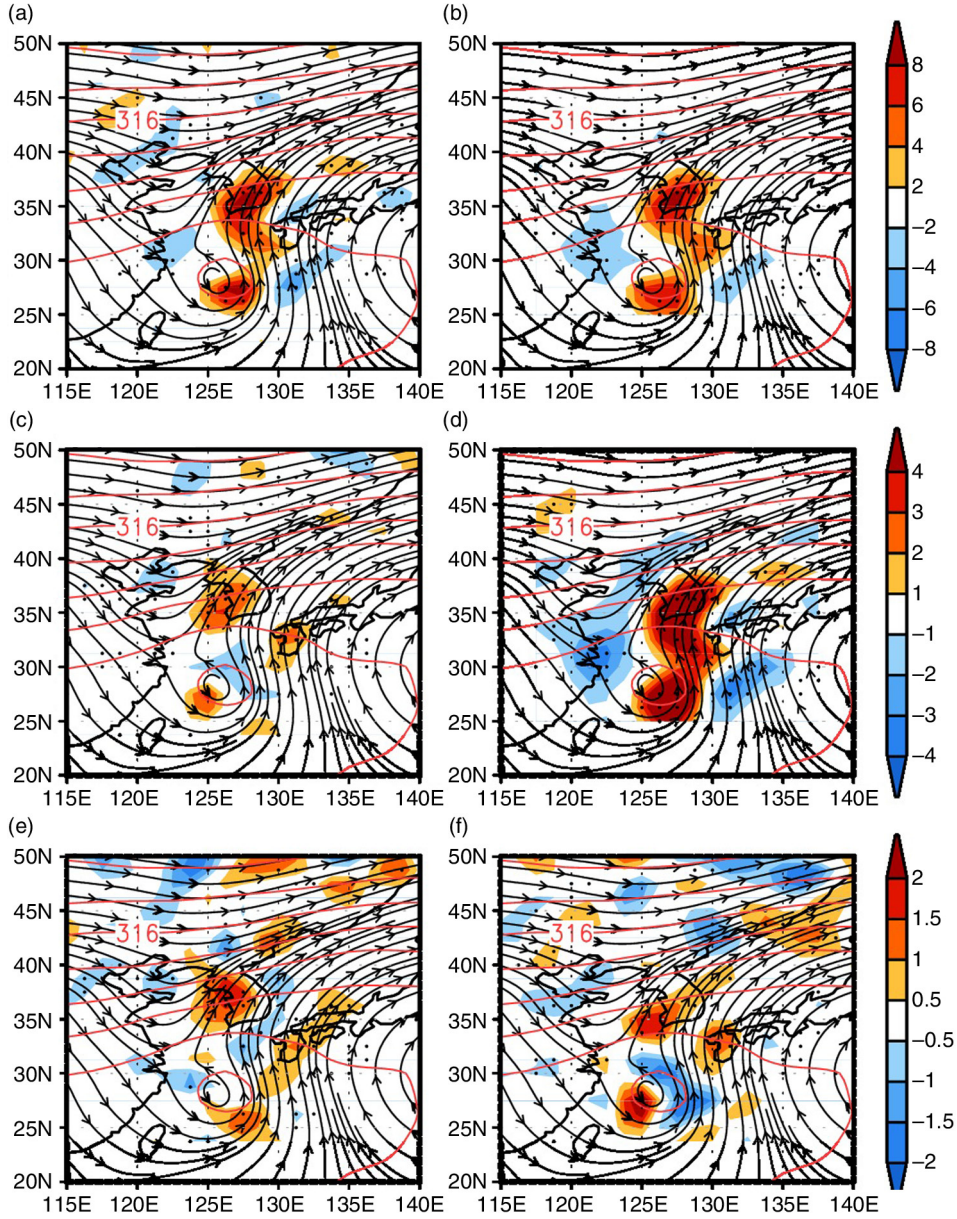*Fig. 7.* Composite fields of various terms of the QG omega equation (shading, units: 10^{-12} Pa m^{-2} s^{-1}) and potential temperature (red contour, units: K) averaged between 700 and 400 hPa. (a) Three-dimensional Laplacian of composite omega [LHS of eq. (3)], (b) sum of all forcing terms [RHS of eq. (3)] (total forcing), (c) sum of QG forcing terms, (d) diabatic forcing terms, (e) differential geostrophic vorticity advection term and (f) the Laplacian of potential temperature advection term.

Equation (4) shows that the vertical motion is forced by the $\overrightarrow{Q}$ convergence because the second term of RHS – the β effect term – is generally small for synoptic-scale motion (Holton, 2004). Indeed, the magnitude of the $\overrightarrow{Q}$ convergence in the AIP composite is very similar to that of the sum of the two QG forcings (Figs. 6b vs. 7c).

The magnitude of the diabatic forcing is generally larger than that of the dynamic forcing, mainly due to precipitation and cloudiness during a rainfall event (Martin et al., 1997). Over the KP, the magnitude of the QG forcing is also smaller than that of the diabatic heating term. However, the QG forcing is as important as the diabatic heating for the upward motion because the latent heat may not be effectively released without condensation that results from vertical motion. We propose the following hypothesis of vertical motion–precipitation feedback exclusively for the ascending motion of the AIP cases over the KP. The upward motion on the warm side of the QG front induces a

release of condensational heat. The diabatic heating forcing again intensifies the upward motion. During the feedback process, the condensate falls out as precipitation, but the moisture supply from the Tropics is enough to sustain the feedback process.

The QG forcing is divided into differential geostrophic vorticity advection (Fig. 7e) and the Laplacian of potential temperature advection (Fig. 7f). In the AIP composite, the upper-level trough intrudes into the northwest of the KP, but no low-pressure system occurs at the low level below the upper-level trough (Fig. 5e). The different flow patterns at different vertical levels produce positive differential geostrophic vorticity advection over the region of interest. The potential temperature advection occurs due to the southerlies that originate from the TC. As a result, the upward motion by the QG forcing is induced at the mid-level as a result of the interaction between the TC and upper-level trough.

5. Contributing factors to AIP

5.1. Moist process

Many studies about the distant rainfall event ahead of a TC (e.g. Stohl et al., 2008; Wang et al., 2009; Chen et al., 2010; Galarneau et al., 2010; Schumacher et al., 2011) have noted that deep moisture transport is a key requirement for heavy rainfall. The AIP cases here also show that deep moisture is transported from the Tropics to the rainfall region through the conduit between the TC and subtropical high (Fig. 8). The deep moisture flux strongly converges at the AIP region over the KP, which indicates that the warm south-erlies dump abundant tropical moisture there (Fig. 8a). In the cross-section along the cross-frontal line (i.e. along 127.5°E), the strong meridional moisture flux convergence ranges from the northern periphery of TC to the AIP region in the low and middle tropospheric layers (Fig. 8b). The abundant moisture pumped from the Tropics is a critical requirement for heavy AIP.

The strong moisture transport and warm advection by the southerlies destabilise the air column in the low and middle tropospheric layers over the AIP region. The convective instability is amplified by the strong transport of warm and moist air from the TC in some RREs (Byun and Lee, 2012). Similarly, the convective instability (measured by the equivalent potential temperature difference between 500 and 850 hPa) increases in the low and middle tropospheric layers in the AIP cases (not shown). The intrusion of warm and moist air provides a convectively unstable environment that supports deep convection over the AIP region.

5.2. Contribution of midtropospheric frontogenesis

The major frontogenesis occurs at the midtropospheric levels from 700 to 400 hPa above the KP, with a relatively strong gradient of potential temperature (Fig. 9). Strong ascent on the warm side of the midtropospheric front
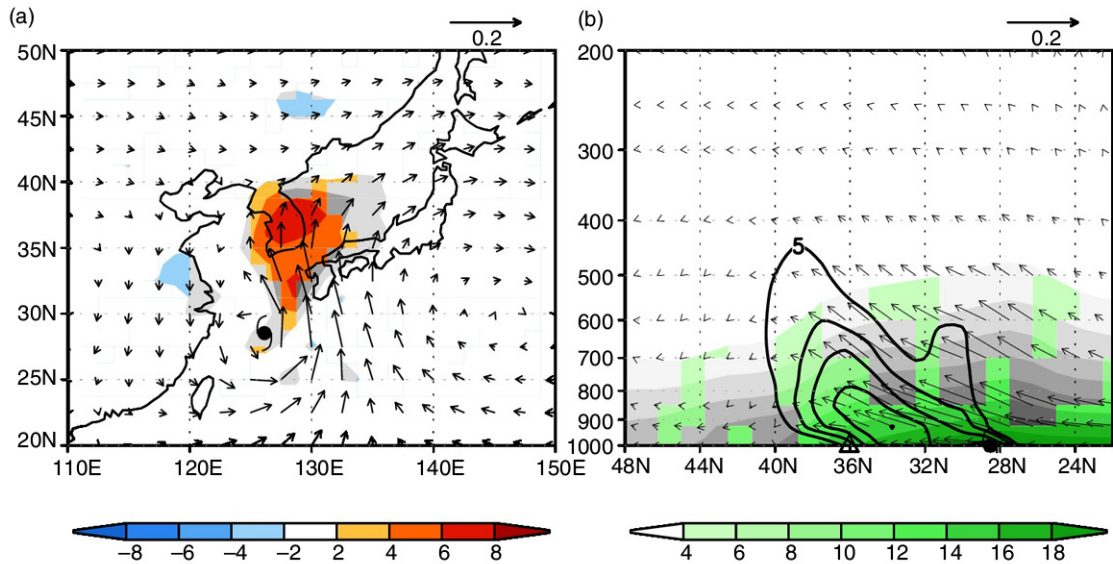

Fig. 8. Composite fields of (a) moisture flux (vector, units: m s^{-1}) and its convergence (shading, units: s^{-1}) averaged between 900 and 500 hPa at the analysis time, (b) meridional–vertical cross-section of specific humidity (shading, units: g kg^{-1}), moisture flux (vector) by meridional wind components (units: m s^{-1}) and negative pressure velocity (units: $30 \times$ Pa s^{-1}), and meridional moisture flux convergence (contour, units: s^{-1}) along 127.5°E. Colour and green shadings denote the 90% significant region of the shading by Student's *t*-test. The TC symbol indicates the composite TC location and the triangle in (b) indicates the mean latitude (36.04°N) of surface stations in South Korea (i.e. the AIP region).
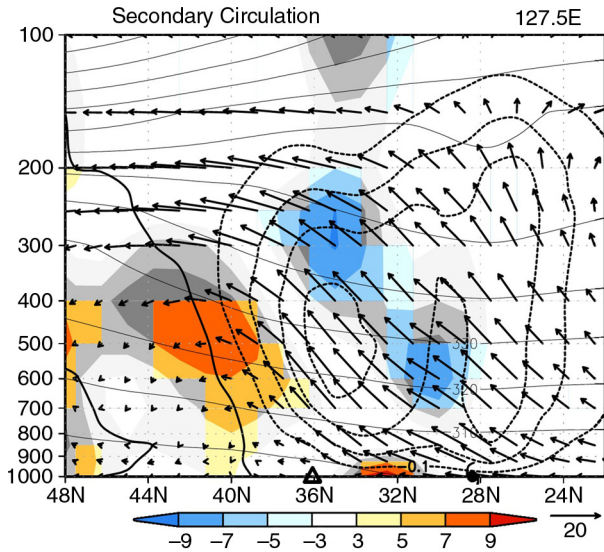
Fig. 9. Meridional–vertical cross-section of total frontogenesis (shading, units: $10^{-11}\,\mathrm{K\,m^{-1}s^{-1}}$), potential temperature (thin contours, units: K) and pressure velocity (thick contours, units: $\mathrm{Pas^{-1}}$) along 127.5°E. Arrows indicate the flow parallel to the cross-section (the horizontal component in $\mathrm{m\,s^{-1}}$ and vertical component in $30\,\mathrm{Pas^{-1}}$). Colour shadings denote the 90% significant region by Student's *t*-test. The TC symbol and triangle are the same as in Fig. 8.

exists at the mid-level, distinctly away from the TC at about 28°N. Induction of the thermally direct circulation can be expected when a positive frontogenesis function occurs in the midtroposphere (Martin et al., 1992; Baek et al., 2013, 2014). The frontogenetical thermally direct circulation can help to enhance the convection and AIP over the KP, with the convective instability of warm and moist air transported along the conduit between the TC and subtropical high. On the other hand, surface frontogenesis also appears on the northern periphery of the TC (about 32°N) during its extratropical transition. However, this surface frontogenesis locates to the south of the rainfall region and, therefore, does not seem to be directly responsible for the AIP event. It should be noted that this surface frontogenesis is not the type observed in association with the PRE in the US (e.g. Moore et al., 2013) but is more relevant to the convergence and resultant deformation downstream of the TC. These features are key differences between the PREs and our AIP cases. The possible reason will be discussed in the next section.

Frontogenesis, ascent and precipitation are linearly related at the analysis time (Fig. 10). The high linear correlation of about 0.75 between precipitation and midtropospheric ascent indicates that the amount of precipitation tends to be proportional to the vertical scale of convection (Fig. 10a). The correlations of the QG frontogenesis north of the KP

with the ascent and precipitation over the KP are reduced to about 0.45 and 0.54, respectively, but are still statistically significant ($p < 0.05$; Fig. 10b and c). These correlation coefficients indicate that about 20% of the ascent and 29% of the precipitation over the KP are explained by the QG frontogenesis. There are larger remaining portions of the variability that are not explained by the QG forcing. However, given the complex nature of vertical motion and precipitation over the mountainous land such as the KP, these statistically significant correlations with the midtropospheric QG frontogenesis imply that the QG approach is effective to understand the AIP event. This is somewhat surprising in the sense that the QG approximation omits many frontogenetical processes (e.g. ageostrophic wind components, tilting and diabatic forcing). Although more complete diagnostics are necessary when individual cases are studied as in Baek et al. (2013, 2014), the QG approximation can be applicable to this kind of climate study using multiple cases that aims to discuss generalised characteristics across them.

To summarise, the abundant transport of tropical moisture by the strong warm advection between the TC and the subtropical ridge destabilises the lower–middle tropospheric layer and acts as a sufficient moisture source, which creates a favourable environment for heavy rainfall. In addition, the thermally direct circulation induced by midtropospheric frontogenesis enhances the upward motion, particularly over the KP. Over the KP, the hypothesised vertical motion–precipitation feedback involving all the above features (Section 4.2) can enhance the convection and precipitation. The essential features are schematically demonstrated in Fig. 11.

6. Discussion: why midtropospheric frontogenesis?

Frontogenesis is a discontinuous phenomenon, so it typically occurs near the surface or tropopause (Bluestein, 1993). However, in our AIP cases, it occurs in the midtroposphere. The different flow patterns at the multilevels may help us to understand the causes of this difference (Fig. 12). The QG frontogenesis function comprised two terms: the divergence term and the resultant deformation term (Keyser, 1988). When a TC approaches the KP, strong cyclonic winds in the vicinity of the TC are predominant at the low level, so that strong convergence and resultant deformation are generated downstream of the TC. This leads to surface frontogenesis north of the TC centre (Fig. 9), but its statistically significant regions are not well organised, that is, they appear sporadically over the domain (Fig. 12c). At the upper level, the flow around the TC is weak, while the strong westerlies and southwesterlies from the mid-latitude
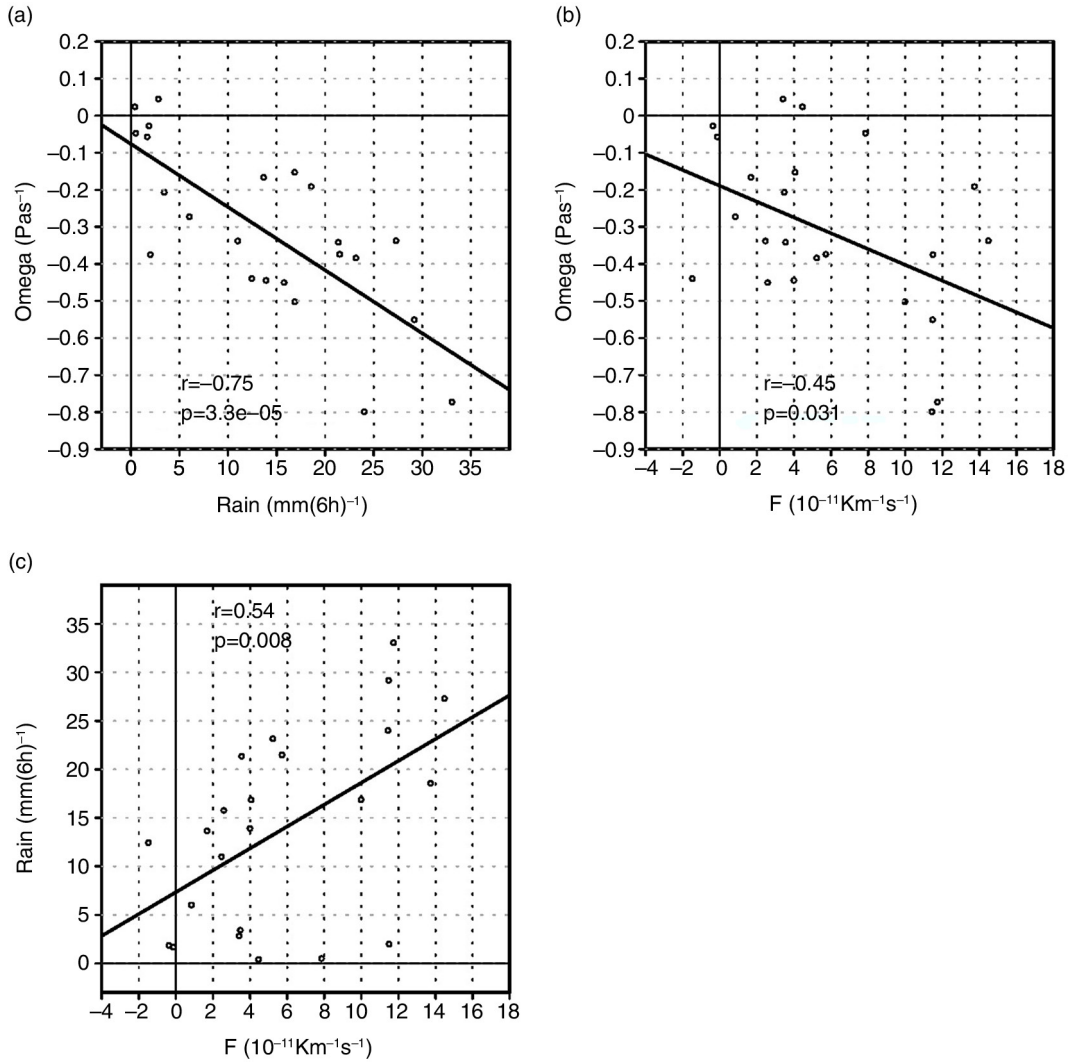
Fig. 10. Scatter plots: (a) between precipitation [units: mm $(6 \text{ h})^{-1}$] averaged for all stations in South Korea and pressure velocity (units: Pas^{-1}) averaged over the ascending region (blue box in Fig. 6a), (b) between QG frontogenesis (units: $10^{-11} \text{ K m}^{-1} \text{ s}^{-1}$) averaged over the frontal region (green box in Fig. 6a) and pressure velocity and (c) between QG frontogenesis and precipitation. All plots use the values at the analysis time.
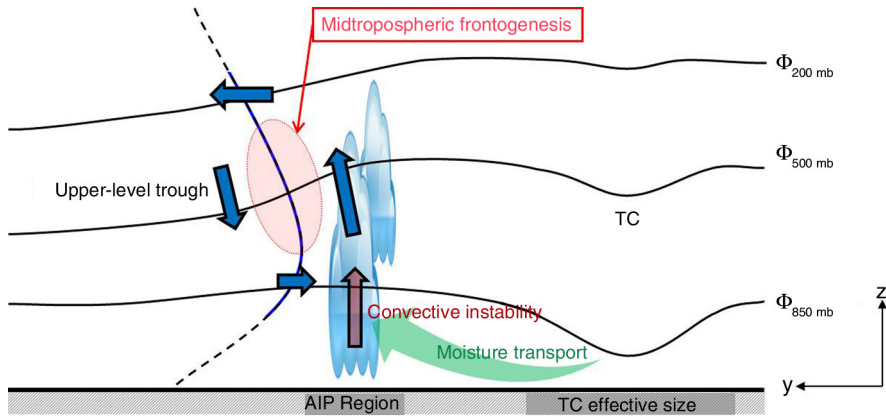

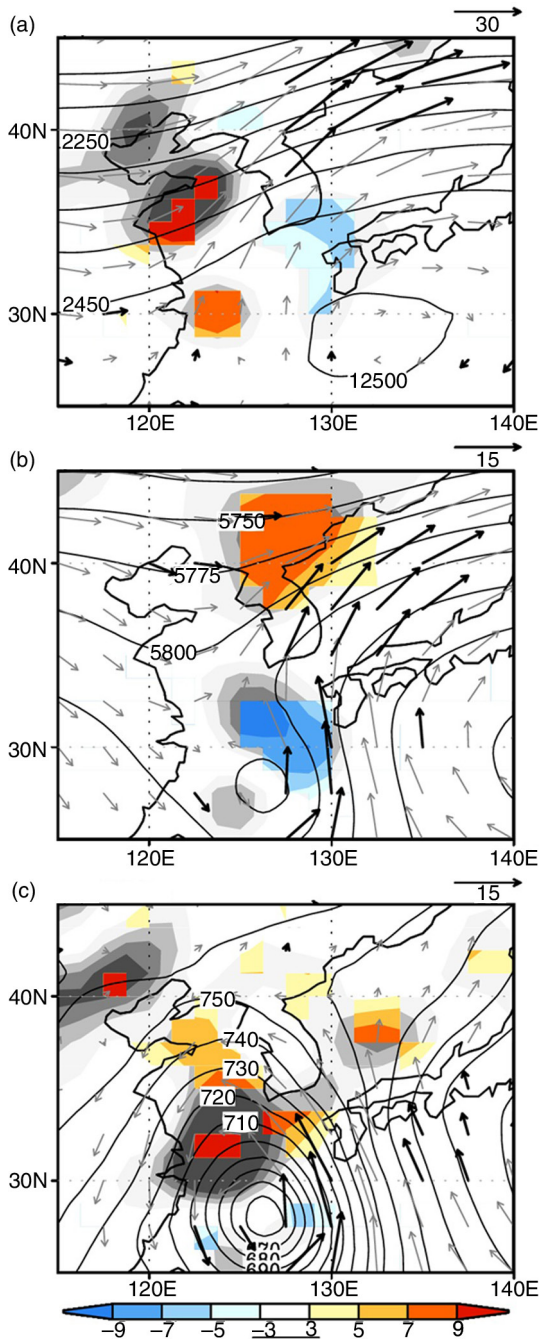*Fig. 11.* Schematic diagram for the physical processes associated with the AIP event over the KP.

Fig. 12. Composite fields of geopotential height (contour, units: gpm), QG frontogenesis [shading, units: 10^{-11}K (m s)$^{-1}$] and horizontal winds (vector, units: m s^{-1}) at (a) 200 hPa, (b) 500 hPa and (c) 925 hPa for the AIP cases at the analysis time. The colour shadings and thick arrows represent the 90% significant region by Student's *t*-test.

trough dominate around the KP (Fig. 12a). However, at the mid-level, the southerlies from the TC collide with the westerlies from the mid-latitude trough with similar strength. This delicate balance causes convergent and deformed flows

in the midtroposphere between the two systems, that is, midtropospheric frontogenesis (Fig. 12b).

In this regard, the results in this study are different from previous studies on the PREs ahead of Atlantic TCs (e.g. Galarneau et al., 2010; Moore et al., 2013) and on the RREs over the KP (e.g. Byun and Lee, 2012). To clarify the difference, we compare the composite patterns of the QG frontogenesis function and multilevel flows at the maximum precipitation time among the AIP, RR-OT and southwesterly jet-cases of the PRE (PRE-SJ; Moore et al., 2013; Fig. 13). Horizontal maps of the AIP composite in Fig. 12 are shown again for convenient contrast. Among the different RRE and PRE categories, the RR-OT and PRE-SJ cases are selected because their synoptic backgrounds share more similarity with the AIP cases. For the composite of PRE-SJ cases, PRE-relative composite analysis is applied following Moore et al. (2013).

For all the cases, the precipitation region is located downstream of the upper-level trough and equatorward of the jet-stream, indicating that all of them are in a baroclinic circumstance (Fig. 13a–c). At the mid-level, the southerly wind component from the TC towards the precipitation region is relatively less prevalent for the RR-OT and PRE-SJ composites; rather, the westerlies blow stronger (Fig. 13d–f). Over the KP, the confluent deformation field where the westerlies and southerlies meet is more conspicuously seen for the AIP composite, compared to the RR-OT composite. Focusing on the upper level, the stronger southwesterly cross-isobaric flow for the AIP composite (Fig. 13a) is an indication of the stronger secondary circulation induced by the confluent deformation at the mid-level (Fig. 9). At the low level (Fig. 13g–i), the averaged TC for the RR-OT composite is located farthest from the precipitating region and the composite TC intensity is weaker. It is noted that the latter is not entirely due to the weaker intensity of TCs but partly attributed to the more spatial spread of TC centres. In the PRE-SJ composite, the region of surface high is more visible to the northwest of the precipitation region (Fig. 13i). As a result, the composite horizontal pattern is more saddle-like at the low level, which could reinforce horizontal stretching deformation.

The differences of composite synoptic background among the three cases are attributed to the different frontogenesis patterns responsible for the precipitation. While the major frontogenesis occurs at the mid-level for the AIP composite, surface frontogenesis is dominant for both the RR-OT and PRE-SJ composites as suggested by previous studies. However, it seems that the surface front forms in different ways between them. In the RR-OT cases, the front primarily originates from the pre-existing surface low-approaching to the precipitation region (as seen in Fig. 2c), not from the flow interaction between the TC and mid-latitude trough because the average TC size is relatively
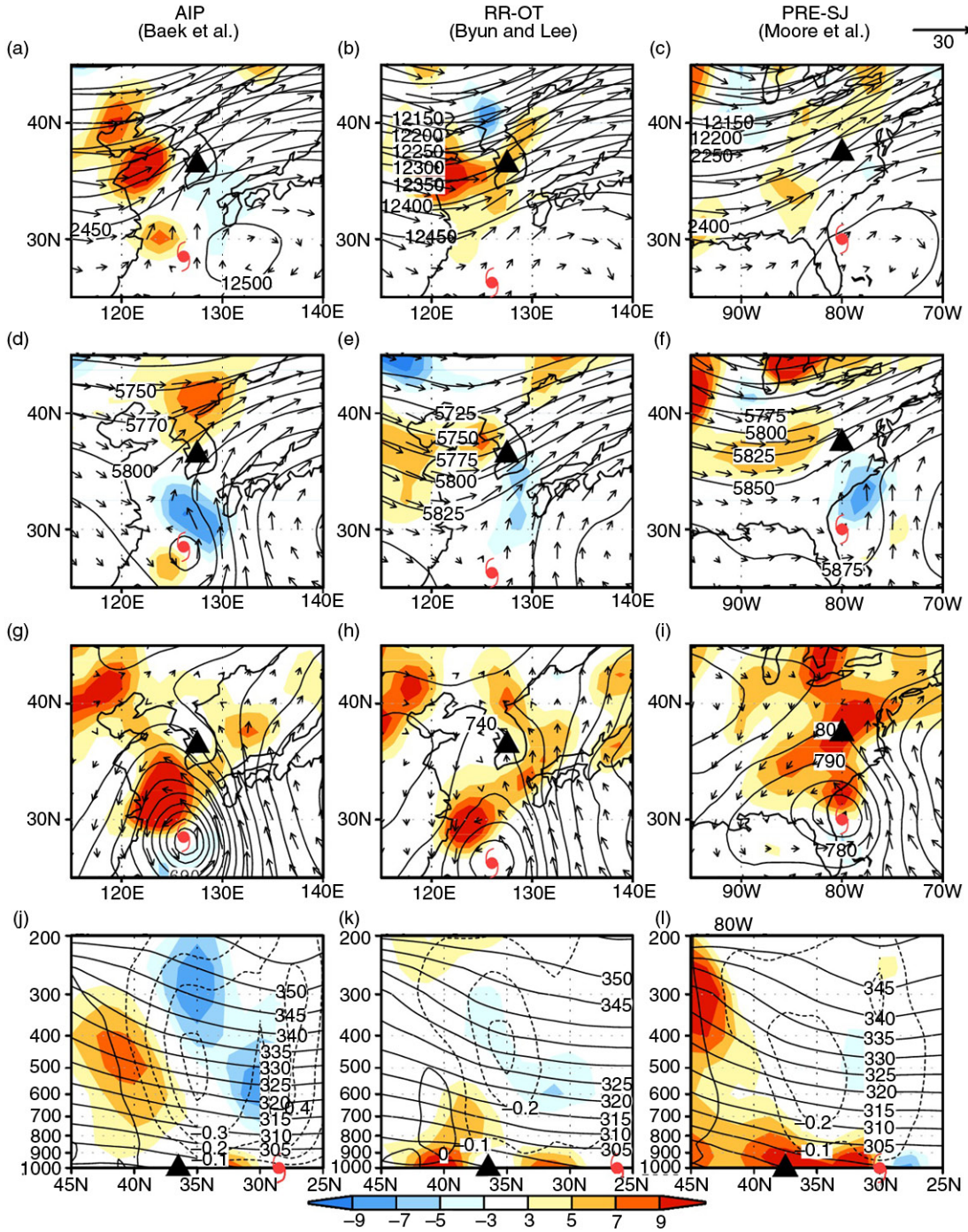
Fig. 13. Geopotential height (contour, units: gpm), QG frontogenesis [shading, units: 10^{-11} K (m s)$^{-1}$] and horizontal winds (vector, units: m s^{-1}) at (a, b, c) 200 hPa, (d, e, f) 500 hPa, and (g, h, i) 925 hPa and (j, k, l) meridional–vertical cross-section of QG frontogenesis, potential temperature (thick contours, units: K) and pressure velocity (thin contours, units: Pa s^{-1}) along 127.5°E at the maximum precipitation time for the composite fields of AIP (left panel), RR-OT (middle panel) and PRE-SJ (right panel), respectively. The black triangle and TC symbol in the bottom panel indicate the precipitating region and composite TC location, respectively.

smaller (discussed in Section 3.3) and the location is also relatively farther from the precipitating region ($\sim$1140 km; c.f. $\sim$880 km for the AIP cases). By contrast, the surface

frontogenesis appears to be induced by the stretching deformation of saddle-shaped flow constituted by the west–east oriented anticyclone couplet (the US continental high and

the Atlantic subtropical high) and the south–north oriented cyclone couplet (the TC and the northern cyclone) for the PRE-SJ cases. Unlike the AIP cases, the flow balances at the low level. These essential differences related to the frontogenesis are more clearly seen in the vertical and latitudinal cross-section across the precipitation region (Fig. 13j–l).

Regarding the contrast between the AIP and PRE-SJ, we think that regional characteristics should also be considered as a possible source of the difference. The North American continent expands further equatorward than does in East Asia; thus, the PRE-related TCs are almost at landfall or have already made landfall when the PRE is initiated (Fig. 6d in Galarneau et al., 2010 and Figs. 1 and 3 in Moore et al., 2013). In such a situation, the Atlantic TC's cyclonic circulation could considerably weaken and transform when the related PRE occurs. This weakening could allow the westerlies induced by the upper-level trough to reach further lower-levels and in turn increase the chance of forming the delicate flow balance. As seen in Fig. 13i and l, the low-tropospheric convergent and deformed flow result in the surface frontogenesis. These distinctive characteristics of the AIP, RR-OT and PRE-SJ are summarised in Table 4.

7. Summary and concluding remarks

Midtropospheric frontogenesis induced by the interaction between the TC and mid-latitude trough was examined to determine its physical significance for the occurrence of AIP over the KP. A set of 41 cases that affected the KP were collected for the period 1993–2004 based on the Typhoon White Book (2011) issued by the KMA. Then, they were classified into AIP (23 TCs) and non-AIP (18 TCs). On average, the AIP occurred about 1 d before the TC made landfall on the KP, and the average maximum 6 h precipitation reached about 116.5 mm.

For the AIP cases, the TC approaching the KP encountered the downstream side of a pre-existing upper-level trough, so a confluent frontal region formed in the midtroposphere. At that time, the equatorward entrance region of an upper-level jet was located over the KP, and the KP was subject to warm and moist air due to the southerlies between the TC and subtropical high. These synoptic features formed a favourable condition for midtropospheric frontogenesis over the KP.

Composite analyses of the AIP cases were conducted to generalise the frontogenetical mechanism and to evaluate the relation between the front and the AIP. Calculation of the QG frontogenesis function showed that the midtropospheric frontogenesis occurred north of the KP. The QG frontogenesis caused $\vec{Q}$ convergence on the warm side of the front (i.e. over the KP) where the ascending motion was strong. Analyses of the QG omega equation enabled us to detect that the ascending motion of the AIP could be attributed to the sum of QG and diabatic forcings. We hypothesise that the vertical motion–precipitation feedback can explain the combined dynamic–thermodynamic processes supportive of deep convection.

The differential flow patterns with vertical levels showed the reason why the AIP-related frontogenesis could occur at the mid-level. The horizontal flows related to the upper-level trough and TC were stronger at the upper level and low level, respectively. The strength of horizontal winds related to the two systems showed the delicate balance at the mid-level, forming the confluent deformation field between the two systems and resulting in the midtropospheric frontogenesis. This frontogenetic feature was in marked contrast to those of the RRE over the KP and the PRE over the US.

A strong moisture flux convergence by the warm southerlies extended to the mid-level with the aid of confluence over the frontal region. The intrusion of warm and moist air at the low-level destabilised the atmosphere and was a major moisture source in the AIP region. The frontogenetical thermally direct circulation further intensified convection over the frontal region ahead of the TC. All these features together helped to intensify the AIP event over the KP. We expect that the results of this study will be useful in the diagnosis and forecast of precipitation associated with TCs approaching the KP.

Table 4. Summary of relevant characteristics of TC and frontogenesis among the AIP, RRE, and PRE cases

	AIP	RR-OT	PRE-SJ
Averaging distance between TC and rainfall region	∼880 km	∼1140 km	∼830 km
TC intensity	Strong	Weak	Weak
Level of wind balance between TC and mid-latitude westerlies	Mid-level	Do not interact	Low level
Frontogenesis	Midtropospheric frontogenesis	Pre-existing surface frontogenesis	Surface frontogenesis

8. Acknowledgements

References

Archambault, H. M., Bosart, L. F., Keyser, D. and Cordeira, J. M. 2013. A climatological analysis of the extratropical flow response to recurving western North Pacific tropical cyclones. *Mon. Weather Rev.* **141**, 2325–2346.

Baek, E.-H., Kim, J.-H., Kug, J.-S. and Lim, G.-H. 2013. Favorable versus unfavorable synoptic backgrounds for indirect precipitation events ahead of tropical cyclones approaching the Korean Peninsula: a comparison of two cases. *Asia-Pacific J. Atmos. Sci.* **49**, 333–346. DOI: 10.1007/s13143-013-0031-0.

Baek, E.-H., Lim, G.-H., Kim, J.-H. and Kug, J.-S. 2014. Antecedent mid-tropospheric frontogenesis caused by the interaction between a tropical cyclone and midlatitude trough: a case study of Typhoon Rusa (2002). *Theor. Appl. Climatol.* **118**, 9–24. DOI: 10.1007/s00704-013-1045-3.

Bluestein, H. B. 1993. *Synoptic-Dynamic Meteorology in Midlatitudes: Vol. II. Observations and Theory of Weather Systems.* Oxford University Press, New York, 608 pp.

Bosart, L. F., Cordeira, J. M., Galarneau, T. J., Jr., Moore, B. J. and Archambault, H. M. 2012. An analysis of multiple predecessor rain events ahead of Tropical Cyclones Ike and Lowell: 10–15 September 2008. *Mon. Weather Rev.* **140**, 1081–1107.

Byun, K.-Y. and Lee, T.-Y. 2012. Remote effects of tropical cyclones on heavy rainfall over the Korean peninsula – statistical and composite analysis. *Tellus.* **64**, 14983. DOI: 10.3402/tellusa.v64i0.14983.

Chen, L., Li, Y. and Cheng, Z. 2010. An overview of research and forecasting on rainfall associated with landfalling tropical cyclones. *Adv. Atmos. Sci.* **27**, 967–976.

Cordeira, J. M. and Bosart, L. F. 2011. Cyclone interactions and evolutions during the "Perfect Storms" of late October and early November 1991. *Mon. Weather Rev.* **139**, 1683–1707.

Galarneau, T. J., Jr., Bosart, L. F., Davis, C. A. and McTaggart-Cowan, R. 2009. Baroclinic transition of a long-lived mesoscale convective vortex. *Mon. Weather Rev.* **137**, 562–584.

Galarneau, T. J., Jr., Bosart, L. F. and Schumacher, R. S. 2010. Predecessor rain events ahead of tropical cyclones. *Mon. Weather Rev.* **138**, 3272–3297.

Hoton, J. R. 2004. *An introduction to dynamic meteorolgy.* Elsevier Academic Press, pp. 168–172.

Keyser, D., Michael, M. J. and Reed, R. J. 1988. A generalization of Petterssen's frontogenesis function and its relation to the forcing of vertical motion. *Mon. Weather Rev.* **117**, 762–780.

Martin, J. E. 2006. Mid-Latitude Atmospheric Dynamics: A First Course. Wiley, pp. 201–204.

Martin, J. E., Locatelli, D. J. and Hobbs, P. V. 1992. Organization and structure of clouds and precipitation on the mid-Atlantic coast of the United States, Part V: The role of an upper-level front in the generation of a rain band. *J. Atmos. Sci.* **49**, 1293–1303.

Martin, M. L., Luna, M. Y. and Valero, F. 1997. Evidence for the role of the diabatic heating in synoptic scale processes: a case study example. *Ann. Geophys.* **15**, 487–493.

Moore, B. J., Bosart, L. F., Keyser, D. and Jurewicz, M. L. 2013. Synoptic environments of predecessor rain events occurring east of the Rocky mountains in association with Atlantic basin tropical cyclones. *Mon. Weather Rev.* **141**, 1022–1046.

Moore, R. W. and Montgomery, M. T. 2005. Analysis of an idealized, three-dimensional diabatic Rossby vortex: a coherent structure of the moist baroclinic atmosphere. *J. Atmos. Sci.* **62**, 2703–2725.

Onogi, K., Tsutsui, J., Koide, H., Sakamoto, M., Kobayashi, S. and co-authors. 2007. The JRA-25 reanalysis. *J. Meteorol. Soc. Jpn.* **85**, 369–432.

Schumacher, R. S., Galarneau, T. J., Jr. and Bosart, L. F. 2011. Distant effects of a recurving tropical cyclone on rainfall in a midlatitude convective system: a high-impact predecessor rain event. *Mon. Weather Rev.* **139**, 650–667.

Stohl, A., Forster, C. and Sodemann, H. 2008. Remote sources of water vapor forming precipitation on the Norwegian west coast at 60°N–a tale of hurricanes and an atmospheric river. *J. Geophys. Res.* **113**, D05102. DOI: 10.1029/2007JD009006.

Wang, Y., Wang, Y. and Fudeyasu, H. 2009. The role of Typhoon Songda (2004) in producing distantly located heavy rainfall in Japan. *Mon. Weather Rev.* **137**, 3699–3716.